PTEP

Prog. Theor. Exp. Phys. **2026** 093B06 (22 pages)
DOI: 10.1093/ptep/ptag159

The Emergence of (3+1)D Expanding Spacetime from Complex Langevin Simulations of the Lorentzian Type IIB Matrix Model with Deformations

Konstantinos N. Anagnostopoulos [1,†], Takehiro Azuma [2,‡], Mitsuaki Hirasawa [3,4,*], Jun Nishimura [5,6,§], Stratos Papadoudis [1,‖], and Asato Tsuchiya [7,¶]

[1]*Physics Department, School of Applied Mathematical and Physical Sciences, National Technical University of Athens, Zografou Campus, GR-15780 Athens, Greece*
[2]*Institute for Fundamental Sciences, Setsunan University, 17-8 Ikeda Nakamachi, Neyagawa, Osaka 572-8508, Japan*
[3]*Department of Physics, Università degli Studi di Milano-Bicocca, Piazza della Scienza 3, I-20126 Milano, Italy*
[4]*Istituto Nazionale di Fisica Nucleare (INFN), Sezione di Milano-Bicocca, Piazza della Scienza 3, I-20126 Milano, Italy*
[5]*KEK Theory Center, Institute of Particle and Nuclear Studies, High Energy Accelerator Research Organization, 1-1 Oho, Tsukuba, Ibaraki 305-0801, Japan*
[6]*Graduate Institute for Advanced Studies, SOKENDAI, 1-1 Oho, Tsukuba, Ibaraki 305-0801, Japan*
[7]*Department of Physics, Shizuoka University, 836 Ohya, Suruga-ku, Shizuoka 422-8529, Japan*

Received June 29, 2026; Accepted August 7, 2026; Published August 14, 2026

The Lorentzian type IIB matrix model is a promising candidate for a nonperturbative formulation of superstring theory. In this model, the eigenvalue distribution of the $N \times N$ bosonic matrices A_μ ($\mu = 0, \ldots, 9$) represents an emergent spacetime, which is determined by the dynamics of the model in the large-N limit. Here we perform numerical simulations of the model overcoming the sign problem by the complex Langevin method with the matrix size N up to 128. In order to avoid the singular drift problem due to the Pfaffian, which appears after integrating out the fermionic matrices, we deform the model in a manner inspired by the supersymmetric deformation, which is used to define the "polarized type IIB matrix model" in the Euclidean case. We find that the deformed model exhibits a phase in which (3+1)D expanding spacetime emerges with both space and time being smooth and real.

Subject Index B83

1. Introduction

The type IIB matrix model [1] (or the IKKT matrix model) is a promising candidate for a nonperturbative formulation of superstring theory. In this model, spacetime [2,3]—as well as gauge fields [4] and matter fields [5,6] on it—is expected to emerge dynamically in the large-N limit.

*mitsuaki.hirasawa@mib.infn.it
†konstant@mail.ntua.gr
‡azuma@mpg.setsunan.ac.jp
§jnishi@post.kek.jp
‖sp10018@central.ntua.gr
¶tsuchiya.asato@shizuoka.ac.jp

© The Author(s) 2026. Published by Oxford University Press on behalf of the Physical Society of Japan. This is an Open Access article distributed under the terms of the Creative Commons Attribution License (https://creativecommons.org/licenses/by/4.0/), which permits unrestricted reuse, distribution, and reproduction in any medium, provided the original work is properly cited.
Funded by SCOAP[3]

Downloaded from academic.oup.com/ptep/article/2026/9/093B06/8761727 by guest on 10 November 2026

Making the matrix size N finite serves as a regularization of the theory analogous to the lattice regularization in gauge theories.

As in lattice gauge theories, Monte Carlo simulations have been used to investigate the dynamical properties of this model. One promising scenario explored up to now is the emergence of a phenomenologically viable cosmology, featuring a (3+1)D expanding spacetime. In this scenario, the extra dimensions remain small due to the dynamics of the model, eliminating the need for additional parameters typically required in conventional compactification scenarios. This raises the possibility that our universe could emerge from the model without encountering the string landscape problem.

The realization of such a scenario was first discussed in Ref. [2] within the context of the Euclidean model. In this model, classical solutions are diagonal up to SU(N) symmetry, and the diagonal elements represent spacetime coordinates. By perturbing around these configurations, it was argued that fermionic zero modes play a crucial role in the dimensional reduction of the emergent spacetime. A nonperturbative study of the Euclidean model [7] based on the Gaussian expansion method demonstrated the spontaneous breaking of the SO(10) rotational symmetry to SO(3). Monte Carlo simulations confirmed this finding [8,9] and highlighted the importance of fermionic dynamics. Integrating out the fermions yields a Pfaffian with a highly oscillatory phase. Its fluctuations are speculated to favor lower-dimensional spaces [10,11]. In the absence of such fluctuations, the rotational symmetry remains unbroken [12–14]. Studies of toy models, employing either the Gaussian expansion method [15,16] or numerical simulations [17–21], have provided further support for this scenario. For a comprehensive review, see Ref. [22].

The Lorentzian model was not investigated until much later due to the severe sign problem arising from the factor e^{iS} in the path integral. The first paper on the Lorentzian model [23] and subsequent papers [24–28] suggested that dominant configurations represent a (3+1)D expanding spacetime. However, Ref. [29] revealed that these configurations possess a singular structure due to an artifact of the approximation employed to circumvent the sign problem. This pointed to the necessity of simulating the model without such approximations. Indeed the complex Langevin method (CLM) [30,31] was used to simulate the bosonic model (i.e. without fermions), and the dominant configurations were found to become smooth as one removes the approximation [32]. Furthermore, it was found that the Lorentzian model with extra quadratic terms [33,34] in the action admits classical solutions representing smooth expanding configurations [6] although the dimensionality of space remains undetermined. Similar deformations also led to other classical backgrounds, where gravity can arise from the one-loop effective action at weak coupling [35–42]. See also Refs. [43–55] for recent related works.

In this paper we attempt to investigate the Lorentzian model with a Lorentz-invariant mass term $S_\gamma = -\frac{N}{2}\gamma \operatorname{Tr}(A_\mu A^\mu)$, where $\gamma > 0$, using the CLM. It is well known that the CLM fails in some cases due to the wrong convergence problem, which can be understood from the arguments for justification [56–61]. In fact, this problem occurs in the present model due to singular drifts from the Pfaffian since some eigenvalues of the associated matrix come close to zero. In order to avoid this problem, we deform the model in a manner inspired by the supersymmetric (SUSY) deformation [62] used to define the polarized type IIB matrix model [63–65] in the Euclidean case.[1] Within a certain parameter regime, we discover a phase in which the space has small extent without spontaneous symmetry breaking (SSB) at early times and three out of

[1]The polarized type IIB matrix model has attracted much attention due to the discovery of holographic dual solutions in type IIB supergravity. See also Refs. [66–69] for Monte Carlo studies.

Downloaded from academic.oup.com/ptep/article/2026/9/093B06/8761727 by guest on 10 November 2026

nine spatial directions start to expand at some point in time. Furthermore, we find that both space and time turn out to be smooth and real. Some preliminary results were presented in Ref. [22] and the proceedings articles in Refs. [70–74]. While the effects of the deformation have to be carefully examined in the next step, our results strongly suggest that the Lorentzian type IIB matrix model has remarkable dynamical properties supporting the scenario for the emergence of (3+1)D expanding spacetime in nonperturbative string theory.

The rest of this paper is organized as follows. In Section 2, we briefly review the Lorentzian type IIB matrix model and explain the motivations to add a Lorentz-invariant mass term. In Section 3, we explain how one can apply the CLM to this model. In Section 4, we present our numerical results obtained by the CLM. Section 5 is devoted to a summary and discussions. In Appendix A, we explain how we remove the artifact of Lorentz boosts, which obscures our analyses of the expanding spacetime. In Appendix B, we discuss the SUSY deformation of the type IIB matrix model in the Lorentzian case to clarify its relationship with the deformation used in the present work.

2. Brief review of the Lorentzian type IIB matrix model

In this section, we briefly review the Lorentzian type IIB matrix model and discuss, in particular, the equivalence to the Euclidean model, which provides the motivation to add a Lorentz-invariant mass term. We also discuss how one can extract the time evolution from a matrix configuration.

2.1. *Equivalence to the Euclidean model*

The action of the type IIB matrix model is given by [1]

$$S = S_{\rm b} + S_{\rm f} \,, \tag{2.1}$$

$$S_{\rm b} = -\frac{1}{4g^2}\mathrm{Tr}\left([A_\mu, A_\nu][A^\mu, A^\nu]\right) \,, \tag{2.2}$$

$$S_{\rm f} = -\frac{1}{2g^2}\mathrm{Tr}\left(\bar{\Psi}_\alpha(\Gamma^\mu)_{\alpha\beta}[A_\mu, \Psi_\beta]\right) \,, \tag{2.3}$$

where A_μ ($\mu = 0, \ldots, 9$) and Ψ_α ($\alpha = 1, 2, \ldots, 16$) are $N \times N$ traceless Hermitian matrices, which transform as a vector and a Majorana–Weyl spinor, respectively, under SO(9,1) transformations. The Lorentz indices are raised and lowered using the Lorentzian metric

$$\eta_{\mu\nu} = \mathrm{diag}(-1, 1, 1, \ldots, 1) \,. \tag{2.4}$$

Γ^μ are the 10D gamma matrices obtained after Weyl projection, and $\bar{\Psi} = \Psi^T \mathcal{C}$, where $\mathcal{C}$ is the charge conjugation operator. We set $g^2 N = 1$ without loss of generality.

The partition function is given by [23]

$$Z = \int dA d\Psi \, e^{i(S_{\rm b}+S_{\rm f})} = \int dA \, e^{iS_{\rm b}} \, \mathrm{Pf}\mathcal{M}(A) \,, \tag{2.5}$$

where $\mathcal{M}$ is a $16(N^2-1) \times 16(N^2-1)$ antisymmetric matrix representing the linear transformation

$$\Psi_\alpha \to (\mathcal{M}\Psi)_\alpha = (\mathcal{C}\Gamma^\mu)_{\alpha\beta}[A_\mu, \Psi_\beta] \,, \tag{2.6}$$

acting on the linear space of traceless complex $N \times N$ matrices Ψ_α. One can easily prove that the Pfaffian $\mathrm{Pf}\mathcal{M}(A)$ is real, unlike the Euclidean case.

Downloaded from academic.oup.com/ptep/article/2026/9/093B06/8761727 by guest on 10 November 2026

Since the integral (2.5) is not absolutely convergent, here we define the model by analytic continuation as follows.[2] Setting $\tilde{S}_{\rm b} = -iS_{\rm b}$ and rewriting the partition function as $Z = \int dA e^{-\tilde{S}_{\rm b}} {\rm Pf}\mathcal{M}(A)$, we have

$$\tilde{S}_{\rm b} = -\frac{i}{4} N \left[-2{\rm Tr}(F_{0i})^2 + {\rm Tr}(F_{ij})^2 \right] , \tag{2.7}$$

where $F_{\mu\nu} = i\big[A_\mu, A_\nu\big]$. The indices i, j run over $1, 2, \ldots, 9$. We consider the contour deformation defined by [32]

$$A_0 = e^{-i\frac{3\pi}{8}u} \tilde{A}_0, \quad A_i = e^{i\frac{\pi}{8}u} \tilde{A}_i \ (i = 1, 2, \ldots, 9) , \quad 0 \le u \le 1, \tag{2.8}$$

where $\tilde{A}_\mu$ are Hermitian. The action (2.7) then becomes

$$\tilde{S}_{\rm b} = \frac{N}{4} \left[2e^{i\frac{\pi}{2}(1-u)} {\rm Tr}(\tilde{F}_{0i})^2 + e^{-i\frac{\pi}{2}(1-u)} {\rm Tr}(\tilde{F}_{ij})^2 \right] , \tag{2.9}$$

where $\tilde{F}_{\mu\nu} = i\,[\tilde{A}_\mu, \tilde{A}_\nu]$. Note that one obtains the Euclidean model at $u = 1$. Here we observe that the coefficients $e^{i\frac{\pi}{2}(1-u)}$ and $e^{-i\frac{\pi}{2}(1-u)}$ have positive real parts for $0 < u \le 1$, and hence the deformed model is well defined in that region. Therefore we define the Lorentzian model by taking the $u \to +0$ limit.

Let us note here that the observable

$$\langle \mathcal{O}(e^{-i\frac{3\pi}{8}u} \tilde{A}_0, \ e^{i\frac{\pi}{8}u} \tilde{A}_i) \rangle_u \tag{2.10}$$

for the action (2.9) is independent of u due to Cauchy's theorem.[3] The $u \to +0$ limit and the $u = 1$ case correspond to the Lorentzian and Euclidean models, respectively. In particular, we obtain the relationship between the two models with respect to the expectation values of ${\rm Tr}(A_0)^2$ and ${\rm Tr}(A_i)^2$ as [70,71]

$$\left\langle \frac{1}{N}{\rm Tr}(A_0)^2 \right\rangle_{\rm L} = e^{-i\frac{3\pi}{4}} \left\langle \frac{1}{N}{\rm Tr}(\tilde{A}_0)^2 \right\rangle_{\rm E} , \quad \left\langle \frac{1}{N}{\rm Tr}(A_i)^2 \right\rangle_{\rm L} = e^{i\frac{\pi}{4}} \left\langle \frac{1}{N}{\rm Tr}(\tilde{A}_i)^2 \right\rangle_{\rm E} , \tag{2.11}$$

where $\langle \cdot \rangle_{\rm L}$ and $\langle \cdot \rangle_{\rm E}$ represent the expectation values in the Lorentzian and Euclidean models, respectively. In Fig. 1, we plot the numerical results of $\left\langle \frac{1}{N}{\rm Tr}(A_0)^2 \right\rangle$ and $\left\langle \frac{1}{N}{\rm Tr}(A_i)^2 \right\rangle$ obtained by applying the CLM, described later in Section 3, to the bosonic model (2.9) without ${\rm Pf}\mathcal{M}(A)$ for $N = 128$. We observe that the relative complex phases for the two quantities are $-\frac{3\pi}{4}$ and $\frac{\pi}{4}$, respectively, which agree with Eq. (2.11).

This implies, in particular, that the emergent spacetime should be interpreted as Euclidean, and moreover it is complex[4] due to the phase factors in Eq. (2.11). Note that the equivalence holds also in the presence of ${\rm Pf}\mathcal{M}(A)$, which implies that all the results[5] obtained for the Euclidean model [22] can be translated trivially as the results for the Lorentzian model.

2.2. *Adding a Lorentz-invariant mass term*

In order to avoid the equivalence to the Euclidean model and hence to define a genuinely Lorentzian model with a real emergent spacetime, we add a Lorentz-invariant mass term to

[2] Note that this procedure breaks Lorentz symmetry. Recently Ref. [75] proposed a new definition of the Lorentzian model, in which the Lorentz symmetry is fixed by the Faddeev–Popov procedure. In that case, the equivalence to the Euclidean model does not hold as demonstrated numerically for $N = 2$ in Ref. [76]. It is considered, however, that the equivalence recovers in the $N \to \infty$ limit since the effect of the Faddeev–Popov determinant is suppressed at large N.

[3] We thank Yuhma Asano for pointing this out to us.

[4] This can happen even if A_μ are Hermitian because of the complex weight $e^{iS_{\rm b}}$ in Eq. (2.5).

[5] For instance, in the Euclidean version of the type IIB matrix model, it has been found that the SO(10) rotational symmetry is spontaneously broken to SO(3), with three dimensions larger than the other seven [7–9], although the physical meaning of this is not clear.

Downloaded from academic.oup.com/ptep/article/2026/9/093B06/8761727 by guest on 10 November 2026

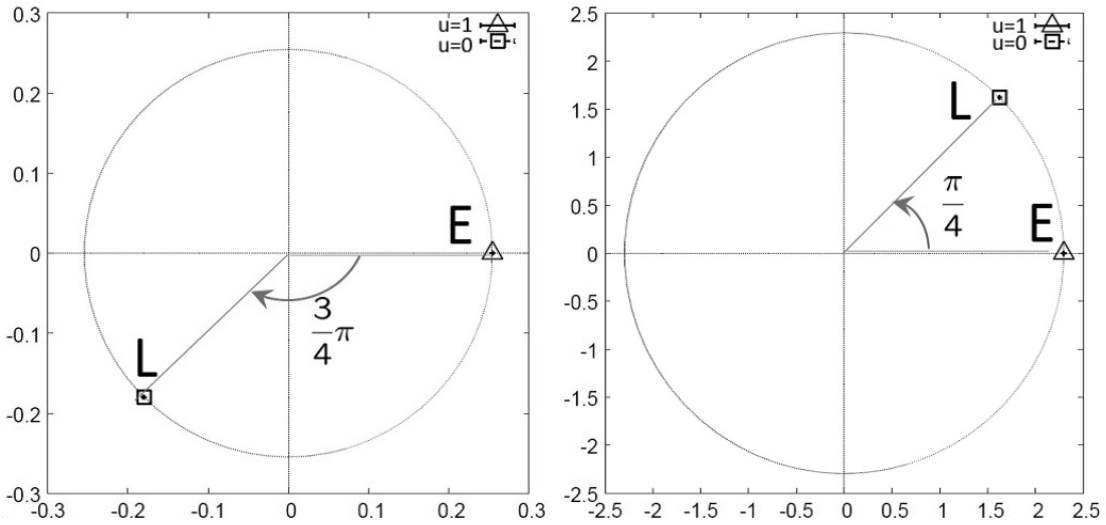

Fig. 1. The expectation values of $\frac{1}{N}\mathrm{Tr}(A_0)^2$ (left) and $\frac{1}{N}\mathrm{Tr}(A_i)^2$ (right) are plotted in the complex plane for the Euclidean (E) and Lorentzian (L) models. The relative complex phases for these quantities are $-\frac{3\pi}{4}$ and $\frac{\pi}{4}$, respectively, which agree with Eq. (2.11) [70,71].

the action given by [22,71–74]

$$S_\gamma = -\frac{N}{2}\gamma\,\mathrm{Tr}(A_\mu A^\mu) = \frac{N}{2}\gamma\,\{\mathrm{Tr}(A_0)^2 - \mathrm{Tr}(A_i)^2\}\,. \tag{2.12}$$

Setting $\tilde{S}_\gamma = -iS_\gamma$ so that it appears in the partition function as $e^{-\tilde{S}_\gamma}$, we obtain

$$\tilde{S}_\gamma = \frac{N}{2}\gamma\,\{e^{-\frac{i}{4}\pi(2+3u)}\mathrm{Tr}(\tilde{A}_0)^2 + e^{\frac{i}{4}\pi(2+u)}\mathrm{Tr}(\tilde{A}_i)^2\}\,. \tag{2.13}$$

For $\gamma < 0$, the real parts of $\gamma\, e^{-\frac{i}{4}\pi(2+3u)}$ and $\gamma\, e^{\frac{i}{4}\pi(2+u)}$ are positive for $0 < u \leq 1$, allowing the matrices to be rotated from the Lorentzian to the Euclidean model. For $\gamma > 0$, however, the real parts of these coefficients are negative for $0 < u \leq 1$, which implies that the equivalence between the Lorentzian ($u \to +0$) and Euclidean ($u = 1$) models does not hold any longer. Thus we can avoid the equivalence to the Euclidean model for $\gamma > 0$.

The impact of the Lorentz-invariant mass term can already be seen at the level of classical solutions. The classical equation of motion of the Lorentzian type IIB matrix model with the mass term reads

$$[A^\nu, [A_\nu, A_\mu]] - \gamma A_\mu = 0\,. \tag{2.14}$$

For $\gamma = 0$, the solutions consist only of simultaneously diagonalizable A_μ as proved in Appendix A of Ref. [77]. In fact, one can generalize the proof[6] to show that the only solution for $\gamma < 0$ is the trivial one $A_\mu = 0$. For $\gamma > 0$, on the other hand, it was found numerically [6] that nontrivial *real* solutions do exist and they typically represent an expanding spacetime with smooth space and time, although the dimension of space is left undetermined. Thus it is conceivable that the Lorentz-invariant mass term (2.12) with $\gamma > 0$ changes the dynamics of the Lorentzian model drastically, and that the large-N limit followed by the $\gamma \to 0$ limit provides its sensible definition.

Let us also note that $1/\gamma^2$ plays the role of $\hbar$ in quantum theory. This can be seen by rescaling the matrices as $A_\mu \to \sqrt{|\gamma|}A_\mu$, which makes γ^2 an overall factor of the whole bosonic action.

[6]We thank Cheng-Tsung Wang for pointing this out to us.

Downloaded from academic.oup.com/ptep/article/2026/9/093B06/8761727 by guest on 10 November 2026

Therefore, at sufficiently large γ, the dominant configurations are expected to be close to a classical solution, which typically exhibits expanding behavior [6] for $\gamma > 0$ as we reviewed above. The purpose of this work is not only to confirm this expectation by explicit numerical simulations but also to see whether (3+1)D expanding spacetime can be realized in the presence of quantum corrections including the effects of fermions.

2.3. *Extracting the time evolution*

Here we discuss how we can extract the time evolution from matrix configurations A_μ that contribute dominantly to the partition function of the Lorentzian type IIB matrix model with the mass term (2.12). For that, we first choose the SU(N) basis in such a way that A_0 is diagonal and its eigenvalues are arranged in ascending order as [23]

$$A_0 = \mathrm{diag}(\alpha_1, \alpha_2, \ldots, \alpha_N), \quad \alpha_1 < \alpha_2 < \ldots < \alpha_N \,. \tag{2.15}$$

In this basis, it turns out that the spatial matrices A_i typically exhibit a band-diagonal structure.[7] Namely, there exists an integer n such that the moduli of the elements $(A_i)_{ab}$ with $|a-b| > n$ are significantly smaller than those with $|a-b| \leq n$ [24–28], as we will see later by calculating the quantity

$$\mathcal{A}_{ab} = \frac{1}{9}\sum_{i=1}^{9}(A_i)_{ab}(A_i)_{ba} \qquad (a, b = 1, 2, \ldots, N) \,. \tag{2.16}$$

This motivates the introduction of $n \times n$ matrices $\bar{A}_i(t)$ defined as [23]

$$\left(\bar{A}_i\right)_{pq}(t_k) = (A_i)_{k+p,k+q} \,, \tag{2.17}$$

where $p, q = 1, 2, \ldots, n$ and $k = 0, 1, \ldots, N-n$. We define the time t_k as

$$t_k = \sum_{j=1}^{k-1}|\tilde{t}_{j+1} - \tilde{t}_j| \,, \qquad \tilde{t}_k = \frac{1}{n}\sum_{p=1}^{n}\langle\alpha_{k+p}\rangle \,. \tag{2.18}$$

The phase $\theta_a^{(\mathrm{t})}$ of the time difference is defined by

$$\langle\Delta\alpha_a\rangle \propto e^{i\theta_a^{(\mathrm{t})}}, \text{ where } \Delta\alpha_a = \alpha_{a+1} - \alpha_a \,. \tag{2.19}$$

The emergence of real time requires $\theta_a^{(\mathrm{t})} = 0$, whereas for $\gamma = 0$, we obtain a Euclidean spacetime with $\theta_a^{(\mathrm{t})} = -\frac{3\pi}{8}$ due to Eq. (2.11).

Using $\bar{A}_i(t)$ defined in Eq. (2.17), we introduce the following observables. First the extent of space at time t is defined as

$$R^2(t) = \left\langle \frac{1}{n}\mathrm{tr}\sum_{i=1}^{9}(\bar{A}_i(t))^2 \right\rangle = e^{2i\theta_{\mathrm{s}}(t)}|R^2(t)| \,, \tag{2.20}$$

where tr denotes the trace over the $n \times n$ matrices. The emergence of real space requires $\theta_{\mathrm{s}}(t) \sim 0$, whereas for $\gamma = 0$, we obtain a Euclidean spacetime with $\theta_{\mathrm{s}}(t) = \frac{\pi}{8}$. (See Eq. (2.11).)

Next we define the "moment of inertia tensor" at time t as

$$T_{ij}(t) = \frac{1}{n}\mathrm{tr}(\bar{A}_i(t)\bar{A}_j(t)) \,, \tag{2.21}$$

which is a 9×9 real symmetric matrix. The eigenvalues $\lambda_i(t)$ of $T_{ij}(t)$ are arranged in descending order as $\lambda_1(t) > \lambda_2(t) > \ldots > \lambda_9(t)$. Note that $\langle\sum_{i=1}^{9}\lambda_i(t)\rangle$ is equal to $R^2(t)$ defined in

[7] More precisely, the band-diagonal structure appears when the emergent space exhibits an expanding behavior, which can be understood from the bosonic part of the action (2.2). When the eigenvalues of A_i become large, the commutator squared terms prefer simultaneously diagonalizable matrices.

Downloaded from academic.oup.com/ptep/article/2026/9/093B06/8761727 by guest on 10 November 2026

Eq. (2.20). If $\mathrm{Re}\langle\lambda_1(t)\rangle, \ \ldots, \mathrm{Re}\langle\lambda_d(t)\rangle$ are larger than the rest, it indicates spontaneous symmetry breaking from SO(9) to SO(d), implying the dynamical generation of d-dimensional space.

When calculating $\langle\lambda_i(t)\rangle$ using the CLM, we encounter the issue that each eigenvalue $\lambda_i(t)$ breaks holomorphicity as a function of A_i. To circumvent this, we compute the coefficients c_k from $\det(z\mathbf{1}_9 - T(t)) = \sum_{k=0}^{9} c_k z^k$ for each configuration,[8] and calculate $\langle c_k\rangle$. Then, we solve the ninth-order equation $\sum_{k=0}^{9}\langle c_k\rangle z^k = 0$ for z numerically, the solutions of which give a practical estimate of $\langle\lambda_i(t)\rangle$. Error bars can be computed using the standard jackknife method.[9]

In order to investigate the smoothness of the emergent space, we consider the eigenvalues of the $n \times n$ matrix [29]

$$Q(t) = \sum_{i=1}^{9} (\bar{A}_i(t))^2, \tag{2.22}$$

whose eigenvalues provide the radial distribution of the points in space. The eigenvalues $q_p(t)$ ($p = 1, 2, \ldots, n$) of $Q(t)$ are arranged in descending order as $q_1(t) > q_2(t) > \ldots > q_n(t)$. The expectation values $\langle q_p(t)\rangle$ are calculated using the CLM in a way similar to the one used for $\langle\lambda_i(t)\rangle$.

3. Application of the complex Langevin method (CLM)

Monte Carlo simulations of the Lorentzian type IIB matrix model are difficult due to the sign problem. Here we use the CLM [30,31], which has been successfully applied to various systems with the sign problem. It involves formulating stochastic differential equations for complexified variables, which can then be used to calculate expectation values under specific conditions.

3.1. *The basic formulation of the CLM*

Let us consider a model defined by the partition function $Z = \int dx\, w(x)$, where $x \in \mathbb{R}^n$ and $w(x)$ is a complex-valued function. In the CLM, we complexify the variables as $x \to z \in \mathbb{C}^n$, and solve the complex Langevin equation with the Langevin time σ given by

$$\frac{dz_k}{d\sigma} = \frac{1}{w(z)}\frac{\partial w(z)}{\partial z_k} + \eta_k(\sigma)\,. \tag{3.1}$$

The first term on the right-hand side is the "drift term", while the second term represents the real Gaussian noise with a probability distribution proportional to $\exp\bigl(-\frac{1}{4}\int d\sigma \sum_k \eta_k(\sigma)^2\bigr)$.

The solution of the above equation corresponds to the probability distribution $P(z, \bar{z}; \sigma)$, which satisfies the Fokker–Planck equation. Under certain conditions, this distribution converges to a stationary distribution $P(z, \bar{z})$ as $\sigma \to \infty$, and one can prove $\int dz d\bar{z}\, \mathcal{O}(z)P(z, \bar{z}) = \int dx\, \mathcal{O}(x)w(x)$ for an observable $\mathcal{O}(x)$, where the holomorphicity of $w(z)$ and $\mathcal{O}(z)$ plays a crucial role. Then the expectation value of $\mathcal{O}(x)$ can be evaluated as

$$\langle\mathcal{O}(x)\rangle \simeq \frac{1}{\sigma}\int_{\sigma_0}^{\sigma_0+\sigma} d\sigma'\mathcal{O}(z(\sigma'))\,, \tag{3.2}$$

[8] The coefficients c_k are calculated using Vieta's formula. This method was suggested to us by L. L. Salcedo.

[9] Since the configurations generated by the CLM are complexified, $\lambda_i(t)$ calculated for each configuration become complex in general. As an alternative method for evaluating $\langle\lambda_i(t)\rangle$, which cannot be fully justified, we can order them by imposing $\mathrm{Re}\lambda_1(t) > \mathrm{Re}\lambda_2(t) > \ldots > \mathrm{Re}\lambda_9(t)$ and calculate $\langle\lambda_i(t)\rangle$ naively. The results obtained in this way are found to be the same as the ones obtained by the method described above within statistical errors.

Downloaded from academic.oup.com/ptep/article/2026/9/093B06/8761727 by guest on 10 November 2026

after some time σ_0 required for the evolution to reach equilibrium. The above proof of justification may fail for various reasons such as large excursions in the imaginary direction, boundary terms, integration cycles, and the influence of irrelevant saddle points in the complex plane. Significant progress has been made in identifying and addressing these pathologies [56–61,78–83], leading to successful applications of the CLM to numerous cases [84–90]. The CLM was also applied to the Euclidean type IIB matrix model [9,21,22], where results consistent with the Gaussian expansion method [7,16] were obtained.

When we apply the CLM to the Lorentzian type IIB matrix model, we first choose the SU(N) basis by imposing Eq. (2.15) in order to make the extraction of time evolution possible in the subsequent analysis. The crucial idea here is to perform a change of variables [32]

$$\alpha_1 = 0, \quad \alpha_a = \sum_{b=1}^{a-1} e^{\tau_b} \quad \text{for } a = 2, \dots, N \,, \tag{3.3}$$

and introduce new real variables τ_a so that the ordering (2.15) of α_a is enforced automatically. Here we do not care about the tracelessness of A_0 since the trace part is decoupled due to the shift symmetry $A_0 \to A_0 + (\text{const.})\mathbf{1}_N$. Instead, we impose the tracelessness on A_0 after generating configurations by applying the shift $A_0 \to A_0 - \left(\frac{1}{N}\mathrm{Tr}A_0\right)\mathbf{1}_N$. The gauge fixing (2.15) and the change of variables (3.3) introduce an extra term [32]

$$S_{\text{g.f.}} = -\log \prod_{1 \le a < b \le N} (\alpha_a - \alpha_b)^2 - \sum_{a=1}^{N-1} \tau_a \tag{3.4}$$

in the action.

Thus the partition function of the model that we investigate by the CLM is given by

$$Z_{\text{eff}} = \int dA_i d\tau e^{-S_{\text{eff}}}, \quad \text{where } S_{\text{eff}} = -i(S_{\text{b}} + S_\gamma) + S_{\text{g.f.}} - \log \mathrm{Pf}\mathcal{M} \,, \tag{3.5}$$

where S_{b}, S_γ, $S_{\text{g.f.}}$, and $\mathrm{Pf}\mathcal{M}$ are defined by Eq. (2.2) with $g^2 N = 1$, Eq. (2.12), Eq. (3.4), and Eq. (2.5), respectively. The dynamical variables are τ_a, which are real, and A_i, which are traceless Hermitian matrices.

In order to implement the CLM, we complexify τ_a and allow A_i to be general complex traceless matrices. The complex Langevin equations are then given by

$$\frac{d\tau_a}{d\sigma} = -\frac{\partial S_{\text{eff}}}{\partial \tau_a} + \eta_a(\sigma) \,, \quad \frac{d(A_i)_{ab}}{d\sigma} = -\frac{\partial S_{\text{eff}}}{\partial (A_i)_{ba}} + (\eta_i)_{ab}(\sigma) \,, \tag{3.6}$$

where $(\eta_i)_{ab}(\sigma)$ and $\eta_a(\sigma)$ are traceless Hermitian matrices and real numbers, respectively, which are drawn from probability distributions proportional to $\exp\left(-\frac{1}{4}\int d\sigma\, \mathrm{Tr}\,\eta_i(\sigma)^2\right)$ and $\exp\left(-\frac{1}{4}\int d\sigma\, \eta_a(\sigma)^2\right)$, respectively. In practice, Eqs. (3.6) are solved by discretizing σ using the second-order Runge–Kutta method as

$$(A_i)_{ab}(\sigma + \Delta\sigma) = (A_i)_{ab}(\sigma) - \Delta\sigma \left\{ \beta_1 \frac{\partial S_{\text{eff}}}{\partial (A_i)_{ba}}(A(\sigma)) + \beta_2 \frac{\partial S_{\text{eff}}}{\partial (A_i)_{ba}}(A'(\sigma)) \right\} + \sqrt{\Delta\sigma}(\tilde{\eta}_i)_{ab}(\sigma) \,, \tag{3.7}$$

$$(A'_i)_{ab}(\sigma) = (A_i)_{ab}(\sigma) - \Delta\sigma \frac{\partial S_{\text{eff}}}{\partial (A_i)_{ba}}(A(\sigma)) + \sqrt{\Delta\sigma}(\tilde{\eta}_i)_{ab}(\sigma) \,, \tag{3.8}$$

where $\Delta\sigma$ is the step size, set to $\Delta\sigma = 10^{-5}$. The coefficients are chosen as $\beta_1 = \beta_2 = \frac{1}{2}\left(1 + \frac{N}{6}\Delta\sigma\right)$ [91]. The factor $\sqrt{\Delta\sigma}$ arises from the normalization of the noise terms $\tilde{\eta}_i(\sigma)$, which are traceless Hermitian matrices following the probability distribution proportional to

Downloaded from academic.oup.com/ptep/article/2026/9/093B06/8761727 by guest on 10 November 2026

$\exp\left(-\frac{1}{4}\sum_\sigma \mathrm{Tr}\,\tilde{\eta}_i(\sigma)^2\right)$. The same $\tilde{\eta}_i(\sigma)$ is used in Eqs. (3.7) and (3.8). The update of τ_a is performed similarly.

3.2. *Some techniques to make the CLM work*

To obtain reliable results equivalent to the path integral using the CLM, we must address two potential issues. The first is the "excursion problem" [57,58], which arises when A_i deviate significantly from Hermitian matrices, and τ_a become far from real numbers. Gauge cooling [60,92,93] is a technique commonly employed to mitigate the excursion problem. While there is no room for gauge cooling since we have already fixed the gauge as in Eq. (2.15), we have not encountered this problem in the simulations reported in this work.

The second issue is the "singular drift problem" [59,94,95], which arises when the drift terms in the complex Langevin equation (3.6) become excessively large. It was found in Ref. [61] that the CLM is justified when the probability distributions of the drift norms

$$u_\tau = \sqrt{\frac{1}{N^3}\sum_{a=1}^{N-1}\left|\frac{\partial S_{\mathrm{eff}}}{\partial \tau_a}\right|^2}\ ,\ u_A = \sqrt{\frac{1}{9N^3}\sum_{i=1}^{9}\sum_{a,b=1}^{N}\left|\frac{\partial S_{\mathrm{eff}}}{\partial (A_i)_{ba}}\right|^2} \tag{3.9}$$

exhibit exponential or faster decay. All results presented in this paper satisfy this criterion.

A naive application of the CLM to the type IIB matrix model does not work due to the singular drift problem caused by the near-zero eigenvalues of the matrix $\mathcal{M}(A)$ that appears in Eq. (2.5). Since the drift term includes the following contribution:[10]

$$\frac{\partial}{\partial (A_i)_{ba}}\{-\log \mathrm{Pf}\mathcal{M}\} = -\frac{1}{2}\mathrm{Tr}\left(\frac{\partial \mathcal{M}}{\partial (A_i)_{ba}}\mathcal{M}^{-1}\right)\ , \tag{3.10}$$

near-zero eigenvalues of $\mathcal{M}$ can lead to the singular drift problem. Here we avoid this problem by adding a fermionic mass term [9]

$$S_{m_{\mathrm{f}}} = -i\, m_{\mathrm{f}}\, \frac{N}{2}\,\mathrm{Tr}\bar{\Psi}(\Gamma^7(\Gamma^8)^\dagger\Gamma^9)\Psi\ , \tag{3.11}$$

which modifies the matrix $\mathcal{M}(A)$ accordingly. Note that the form of Eq. (3.11) is chosen so that the Lorentz symmetry SO(9, 1) is broken minimally to SO(6, 1) × SO(3). One can also prove that the Pfaffian is real for $m_{\mathrm{f}} \in \mathbb{R}$. The effect of fermionic matrices diminishes with increasing m_{f}, and in the $m_{\mathrm{f}} \to \infty$ limit, the fermionic matrices decouple completely, resulting in the bosonic model. For real m_{f}, this term shifts the eigenvalues of $\mathcal{M}(A)$ away from the origin in the real direction, as can be seen in Fig. 2.

In fact, it turns out to be challenging to make m_{f} smaller than some value. As we lower m_{f}, the computational cost increases due to slower convergence of the conjugate gradient method used to evaluate Eq. (3.10). Furthermore, some of the eigenvalues of $\mathcal{M}(A)$ approach the origin, causing the singular drift problem. The distributions of the drifts in Eq. (3.9) develop long tails that decay as a power of u_τ or u_A, failing to satisfy the criterion proposed in Ref. [61], and hence the CLM becomes unreliable.

Keeping m_{f} sufficiently large to ensure reliable results suppresses the contributions from fermion matrices. In order to compensate for this suppression and to investigate the influence

[10] This trace is calculated for the $16(N^2-1)\times 16(N^2-1)$ matrix using the "noisy estimator". See Appendix A of Ref. [21] for details. The noisy estimator involves solving the linear equation $\mathcal{M}\vec{x} = \vec{b}$, where $\vec{x}$ and $\vec{b}$ are $16(N^2-1)$D vectors, using the conjugate gradient (CG) method. Preconditioning with the input vector $\vec{x}_0 = \frac{1}{m_{\mathrm{f}}}\vec{b}$ reduces the required CG iterations by approximately 10% compared to using the naive input vector $\vec{x}_0 = \vec{0}$.

Downloaded from academic.oup.com/ptep/article/2026/9/093B06/8761727 by guest on 10 November 2026

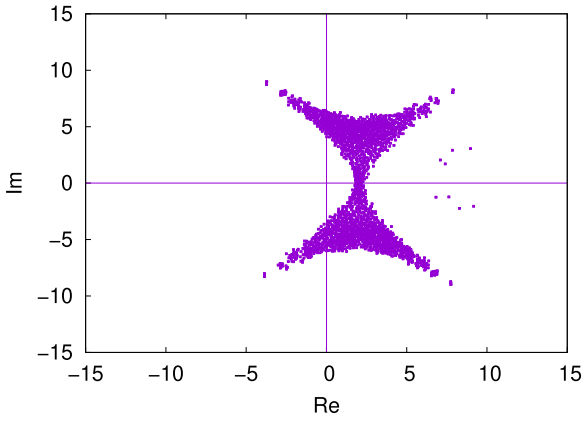

Fig. 2. The eigenvalues of the matrix $\mathcal{M}$ obtained for $N = 16$, $\gamma = 6$, $\tilde{d} = 6$, $\xi = 18$, and $m_{\rm f} = 2$, where the parameters $\tilde{d}$ and ξ are introduced in Eq. (3.12).

of SUSY on the emergent spacetime, we enhance the fermionic contributions by suppressing bosonic fluctuations. Inspired by a Berenstein–Maldacena–Nastase (BMN)-type deformation [96] of the type IIB matrix model,[11] which preserves SUSY [62], we modify the Lorentz-invariant mass term (2.12) as

$$S_\gamma = \frac{1}{2} N\gamma \left(\mathrm{Tr}\,(A_0)^2 - \sum_{i=1}^{\tilde{d}} \mathrm{Tr}\,(A_i)^2 - \xi \sum_{j=\tilde{d}+1}^{9} \mathrm{Tr}\,\big(A_j\big)^2 \right) , \tag{3.12}$$

where ξ (≥ 1) is an additional parameter introduced to suppress the fluctuations of $(9-\tilde{d})$ bosonic matrices. This term breaks the Lorentz symmetry from SO(9,1) to SO($\tilde{d}$, 1). See Appendix B for the relationship of our deformations (3.11) and (3.12) with the SUSY deformation.

An additional technique to stabilize the simulation involves inserting the procedure

$$A_i \mapsto \frac{A_i + \eta A_i^\dagger}{1+\eta} \quad \text{for } i = 1, \ldots, 9 , \tag{3.13}$$

after each Langevin step, where the real positive parameter η should be chosen as small as possible. This technique is similar to the dynamical stabilization employed in lattice QCD applications of the CLM although its justification is not rigorous [97]. Note that $\eta = 1$ corresponds to enforcing hermiticity on A_i. In the following, we set $\eta = 0.005$.

4. Results of the complex Langevin simulations

In this section we present our numerical results obtained by the CLM. First we show our results for the bosonic model, where the fermionic matrices are omitted by hand. While we observe an expanding behavior, we find no SSB of the rotational SO(9) symmetry. Then we show our results for the SUSY model with some deformation inspired by the SUSY deformation [62]. We find a phase with (3+1)D expanding spacetime, where only three out of nine directions start to expand at some point in time. Unlike the previous results [23–28] with singular spatial structure [29], we find that the space is not only real but also smooth.

4.1. *Results for the bosonic model*

Figure 3 shows the expectation values of the eigenvalues α_a of the temporal matrix A_0 and the eigenvalues $\lambda_i(t)$ of $T_{ij}(t)$ for the bosonic model with the Lorentz-invariant mass term (2.12)

[11] See Ref. [66–69] for Monte Carlo studies of the Euclidean model with this SUSY deformation.

Downloaded from academic.oup.com/ptep/article/2026/9/093B06/8761727 by guest on 10 November 2026

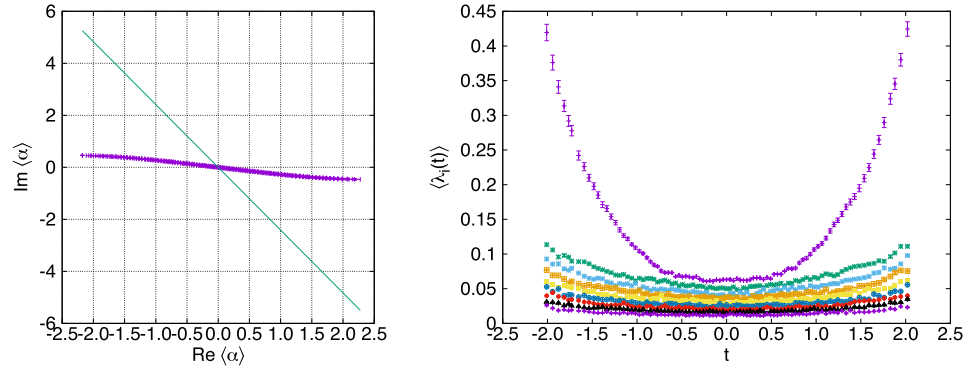

Fig. 3. (Left) The expectation values $\langle\alpha_a\rangle$ of the eigenvalues of the temporal matrix A_0 are plotted in the complex plane for the bosonic model with $N = 96$, $n = 6$, and $\gamma = 4$. The solid line represents the behavior (2.19) expected for the original Lorentzian model ($\gamma = 0$). (Right) The real parts of $\langle\lambda_i(t)\rangle$, the expectation values of the eigenvalues of $T_{ij}(t)$, are plotted against time for the same model.

for $N = 96$, $n = 6$, and $\gamma = 4$, where n is the block size used in Eq. (2.17) and γ is the coefficient of the mass term (2.12). The initial configuration is chosen randomly by generating Gaussian variables for each element of the matrices. The near-horizontal distribution of $\langle\alpha_a\rangle$ at late times (large $|\alpha_a|$) indicates the emergence of real time. We find that one of the nine eigenvalues of $T_{ij}(t)$ grows with t. While this was misinterpreted as evidence for the emergence of an expanding (1+1)D spacetime in our earlier proceedings articles [72,73], it was noticed in Ref. [74] that it is actually an artifact of Lorentz boosts. Since the model has Lorentz symmetry, the configurations are Lorentz boosted as the simulation proceeds, which implies that we have to be careful when we interpret A_0 and A_i as time and space, respectively, as we did in Section 2.3.

To assess the impact of the Lorentz boosts, we measure[12]

$$X_i(t_a) = \frac{1}{n}\, s_i\, \mathrm{tr}\bar{A}'_i(t_a)\,, \qquad \bar{A}'_i(t) = \sum_{j=1}^{9} O_{ij}\bar{A}_j(t) \tag{4.1}$$

at each time t_a ($a = 0, 1, 2, \ldots, N - n$), where we do not sum over i, and O is a 9×9 orthogonal matrix defined by

$$\tilde{\Lambda} = O\,\tilde{T}\,O^{\top}\,,$$
$$\tilde{T}_{ij} = \frac{1}{N}\mathrm{Tr}(A_iA_j)\,, \tag{4.2}$$

where $\tilde{\Lambda} = \mathrm{diag}(\tilde{\lambda}_1, \tilde{\lambda}_2, \ldots, \tilde{\lambda}_9)$ is a diagonal matrix with $\tilde{\lambda}_1 > \tilde{\lambda}_2 > \ldots > \tilde{\lambda}_9$. This quantity (4.1) represents the trace of each spatial block matrix in the SO(9) basis that diagonalizes the moment of inertia tensor $\tilde{T}$ for the whole spacetime. The sign s_i is defined by $s_i = \mathrm{sgn}\{\mathrm{tr}\bar{A}'_i(t_{N-n})\}$, associated with the latest time $t = t_{N-n}$. This is needed since otherwise the expectation value of Eq. (4.1) becomes trivially zero due to the $\mathbb{Z}_2$ symmetry ($A_i \to -A_i$).

[12]Strictly speaking, the quantity (4.1) and all the observables measured after the Lorentz transformation discussed below are not holomorphic, which obscures their physical meaning in the CLM. However, we consider that this is not a serious issue given that the configurations A_μ obtained by complex Langevin simulations turn out to be close to Hermitian. (See Figs. 7 (left) and 8.) Let us also note that, for A_i in Eqs. (4.1) and (4.2), we actually use the Hermitian part $(A_i + A_i^\dagger)/2$ of the configurations generated by the CLM, which is justified only approximately. Ideally, we should perform simulations of the Lorentzian model after fixing the Lorentz symmetry [75,76], which is now ongoing.

Downloaded from academic.oup.com/ptep/article/2026/9/093B06/8761727 by guest on 10 November 2026

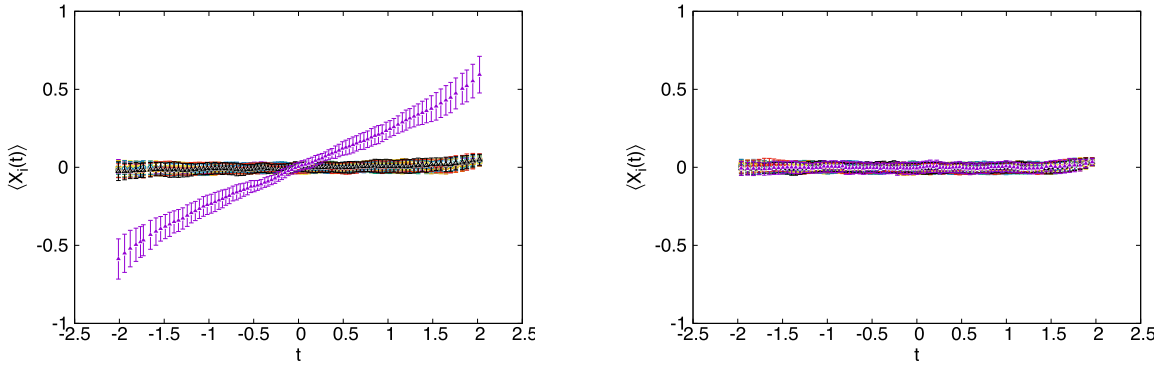

Fig. 4. (Left) $\langle X_i(t)\rangle$ defined by Eq. (4.1) is plotted against time for the bosonic model with $N = 96$, $n = 6$, and $\gamma = 4$ before the Lorentz transformations. Different colors correspond to different indices i. (Right) $\langle X_i(t)\rangle$ is plotted against time for the same model after the Lorentz transformations.

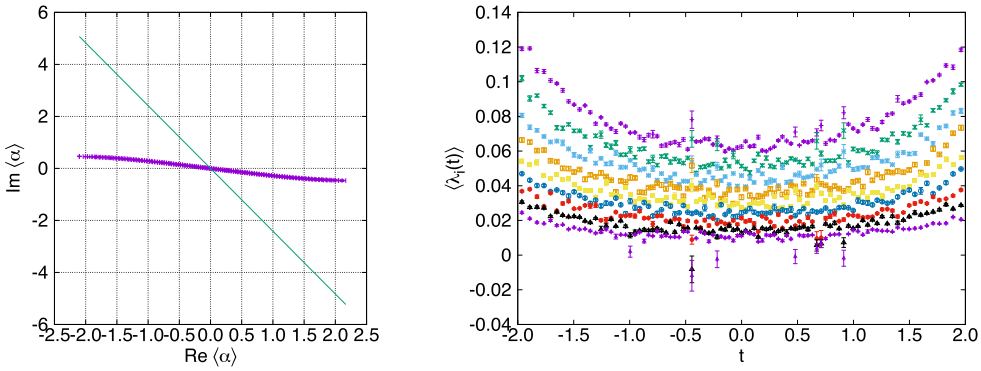

Fig. 5. The same as Fig. 3 except that the results are obtained after the Lorentz transformations.

In Fig. 4 (left), we plot $\langle X_i(t)\rangle$ for the configurations obtained in the simulation. The result for the direction $i = 1$ exhibits linear growth in time, indicating that the obtained configurations are Lorentz boosted. Therefore, we must remove the artifact of Lorentz boosts to extract the proper information about the emergent spacetime.

Figure 4 (right) shows $\langle X_i(t)\rangle$ after the Lorentz transformations, which are determined in such a way that the "center-of-mass motion" is removed for each configuration. (See Appendix A for the details of the procedure.) Comparing this with Fig. 4 (left), we find that the linear growth of the trace of the block matrices has been eliminated by appropriate Lorentz transformations.

Figure 5 presents the expectation values of the eigenvalues α_a of the temporal matrix A_0 (left) and the eigenvalues $\lambda_i(t)$ of $T_{ij}(t)$ (right) after the Lorentz transformations. This figure should be compared with Fig. 3, which is obtained before the Lorentz transformations. While the eigenvalue distribution of α_a remains largely unaffected by the Lorentz transformations, the nine eigenvalues of $T_{ij}(t)$ converge significantly after the transformations, which indicates that the observed 1D expansion is indeed an artifact of Lorentz boosts.

4.2. *The effects of SUSY*

In the previous section, we observed that the SO(9) symmetry remains unbroken in the bosonic model after removing the artifact of Lorentz boosts. In this section, we perform similar analyses

Downloaded from academic.oup.com/ptep/article/2026/9/093B06/8761727 by guest on 10 November 2026

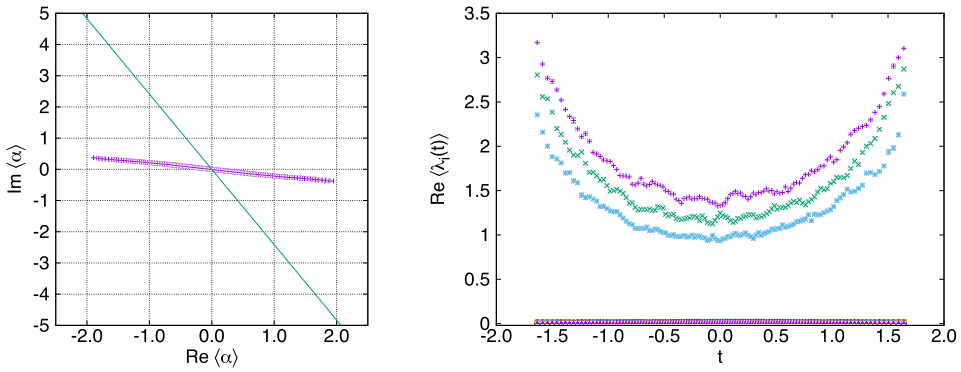

Fig. 6. (Left) The expectation values $\langle \alpha_a \rangle$ of the eigenvalues of the temporal matrix A_0 are plotted in the complex plane for the bosonic model with $N = 128$, $n = 12$, $\gamma = 4$, $\tilde{d} = 3$, and $\xi = 10$. The solid line represents the behavior (2.19) expected for the original Lorentzian model ($\gamma = 0$). (Right) The real parts of $\langle \lambda_i(t) \rangle$, the expectation values of the eigenvalues of $T_{ij}(t)$, are plotted against time for the same model. The thermalized configuration is used as the initial configuration for the subsequent simulations.

in the presence of the contributions from fermionic matrices. In particular, we will see that SUSY plays a crucial role in driving the expansion of three spatial directions.

We begin with a simulation of the bosonic model using the modified mass term (3.12) with $\tilde{d} = 3$ and $\xi = 10$. In Fig. 6, we present the results of this simulation. In the left panel, we show the eigenvalues of A_0. In the right panel, we show the expectation values $\langle \lambda_i(t) \rangle$ of the eigenvalues of $T_{ij}(t)$. The thermalized configuration from this simulation is then used as the initial configuration[13] for simulating the model with fermionic contributions for $N = 128$, $n = 6$, $\gamma = 4$, where we use the SUSY-inspired deformation given by the fermionic mass term (3.11) with $m_{\rm f} = \infty$,[14] 10, 6 and the modified bosonic mass term (3.12) with $\tilde{d} = 5$ and $\xi = 12$. Below we present the results for this deformed model after applying the Lorentz transformations to remove the artifact of Lorentz boosts.

In Fig. 7, we show the results obtained for the $m_{\rm f} = \infty, 10, 6$ cases. From the left panels, we find that the eigenvalue distribution of A_0 becomes parallel to the real axis at late times (in particular, for the smallest $m_{\rm f} = 6$), indicating the emergence of real time in that regime. From the right panels, we find that the SO($\tilde{d}$) rotational symmetry remains unbroken for the $m_{\rm f} = \infty$ and $m_{\rm f} = 10$ cases. In contrast, in the $m_{\rm f} = 6$ case, while the SO($\tilde{d}$) spatial rotational symmetry appears to be preserved at early times close to the origin, it is spontaneously broken to SO(3) at later times.[15] Subsequently, only three eigenvalues exhibit rapid growth. This result provides evidence for a phase in which an expanding (3+1)D spacetime emerges at late times. As we increase $m_{\rm f}$ adiabatically from this configuration, we find that simulations get unstable at $m_{\rm f} = 8$, hinting at a phase boundary in that region.

In Fig. 8, we show that the emergent space is actually real and smooth for the three cases. In the left panel, we present the results for the phase $\theta_{\rm s}(t)$ of the space defined in Eq. (2.20).

[13] Unfortunately, the CLM is not capable of finding the most dominant saddle points. We have to prepare an initial configuration, which is expected to be close to the most dominant saddle point. In order to overcome this weakness of the method, we have to perform simulations with the Lefschetz thimble method as has been done in Ref. [76] for $N = 2$.

[14] By $m_{\rm f} = \infty$, we actually mean the bosonic model, where Pf$\mathcal{M}$ is omitted by hand.

[15] If we start our simulation from a random configuration as we did in the bosonic model, we obtain results similar to those for $m_{\rm f} = 10$. See also footnote 13.

Downloaded from academic.oup.com/ptep/article/2026/9/093B06/8761727 by guest on 10 November 2026

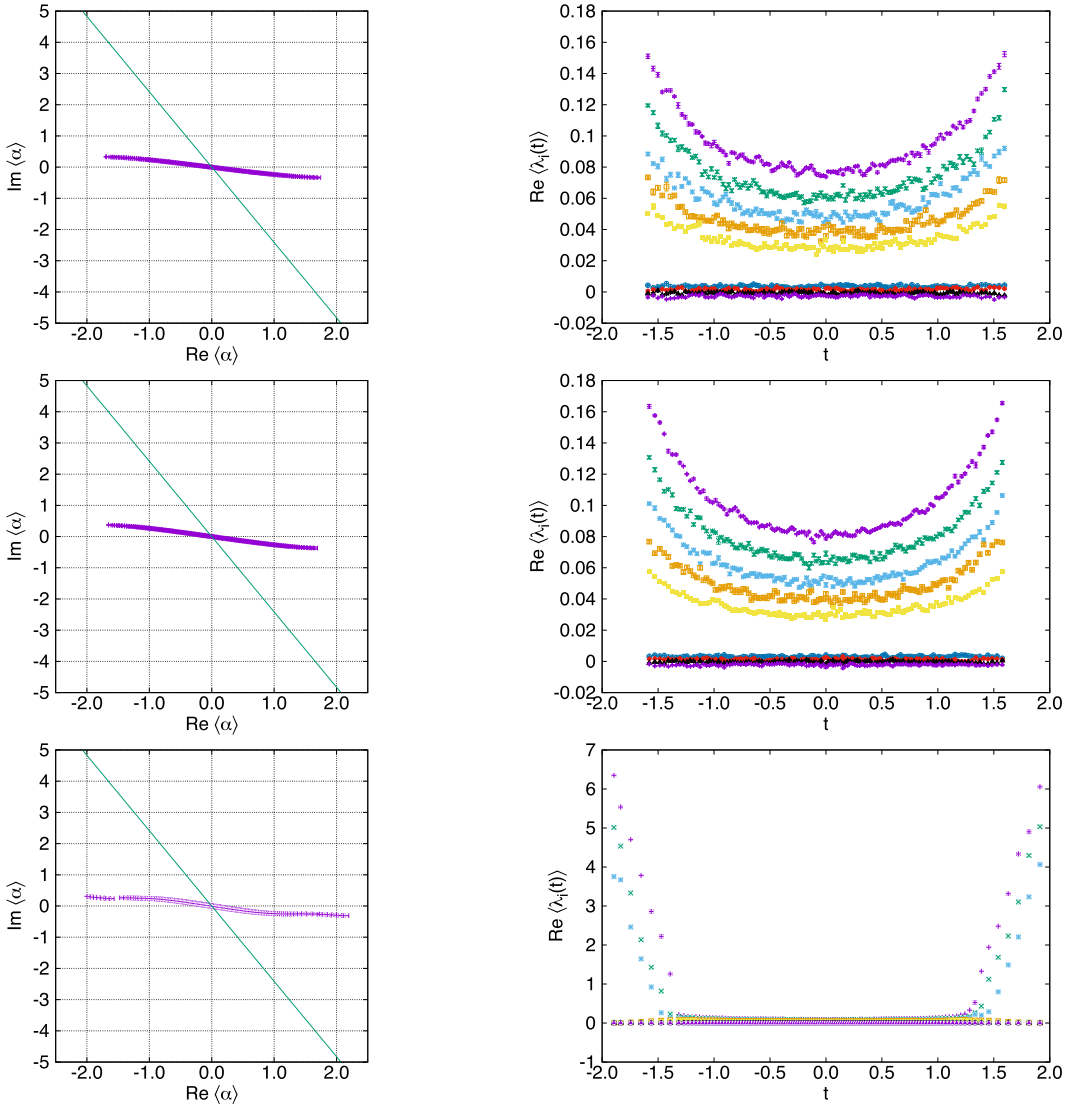

Fig. 7. (Left) The expectation values $\langle \alpha_a \rangle$ of the eigenvalues of the temporal matrix A_0 are plotted in the complex plane for the bosonic model (top), the model with fermionic contributions at $m_{\rm f} = 10$ (middle), and at $m_{\rm f} = 6$ (bottom), with $N = 128$, $n = 6$, $\gamma = 4$, $\tilde{d} = 5$, and $\xi = 12$. The solid line represents the behavior (2.19) expected for the original Lorentzian model ($\gamma = 0$). (Right) The real parts of $\langle \lambda_i(t) \rangle$, the expectation values of the eigenvalues of $T_{ij}(t)$, are plotted against time for the same models.

The horizontal line shows the value $\frac{\pi}{8} \sim 0.39$ for the original Lorentzian model with $\gamma = 0$, which is equivalent to the Euclidean model. The values obtained by simulations are an order of magnitude smaller than this value. In the right panel, we show the results for the real parts of $\langle q_p(t) \rangle$, the expectation values of the eigenvalues of $Q(t)$. We find that the eigenvalues are densely distributed, unlike the case in which we find singular structure described by Pauli matrices [29].

Figure 9 shows the quantity $\mathcal{A}_{ab}$ defined by Eq. (2.16) for the three cases, illustrating the band-diagonal structure of the spatial matrices, which plays a crucial role in extracting the time evolution as we discussed in Section 2.3.

Downloaded from academic.oup.com/ptep/article/2026/9/093B06/8761727 by guest on 10 November 2026

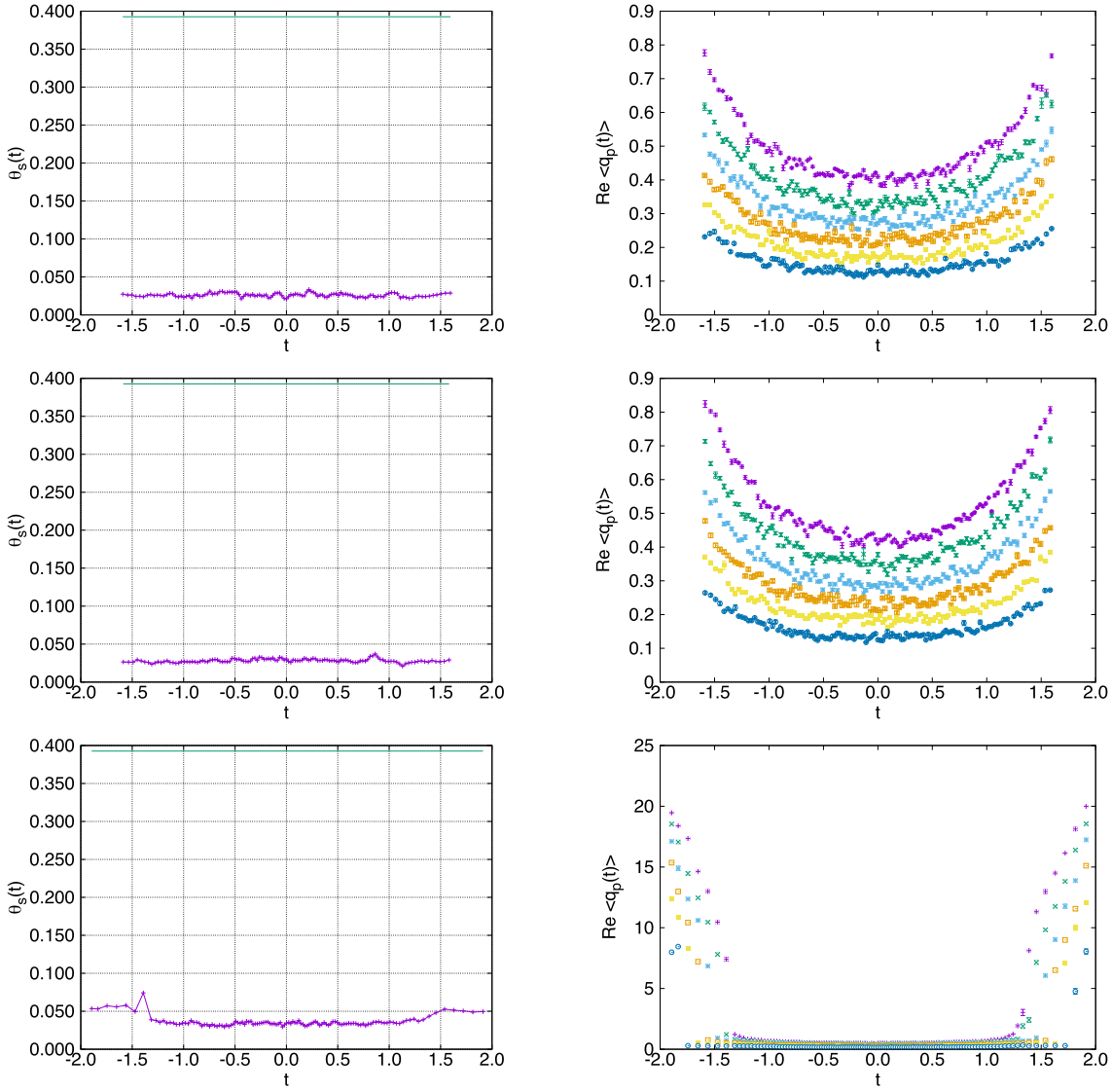

Fig. 8. (Left) The phase of space $\theta_s(t)$ is plotted for the bosonic model (top) and for the model with fermionic contributions at $m_f = 10$ (middle) and at $m_f = 6$ (bottom), with $N = 128$, $n = 6$, $\gamma = 4$, $\tilde{d} = 5$, and $\xi = 12$. The horizontal line shows the value $\frac{\pi}{8} \sim 0.39$ for the original Lorentzian model with $\gamma = 0$, which is equivalent to the Euclidean model. (Right) The real parts of $\langle q_p(t) \rangle$, the expectation values of the eigenvalues of $Q(t)$, are plotted against time for the same models.

5. Summary and discussions

In this paper, we investigated the Lorentzian version of the type IIB matrix model, a proposed nonperturbative formulation of superstring theory, employing the CLM to address the sign problem with matrix size $N \leq 128$. First we established the equivalence between the Lorentzian and Euclidean versions of the type IIB matrix model under a contour deformation. Consequently, one cannot obtain spacetime with a Lorentzian signature from the original model, which motivated us to introduce a Lorentz-invariant mass term (2.12) in the action with $\gamma > 0$. Indeed, for sufficiently large γ, the dominant configurations exhibit the emergence of an expanding spacetime with the Lorentzian signature as expected from the classical analysis [6].

Downloaded from academic.oup.com/ptep/article/2026/9/093B06/8761727 by guest on 10 November 2026

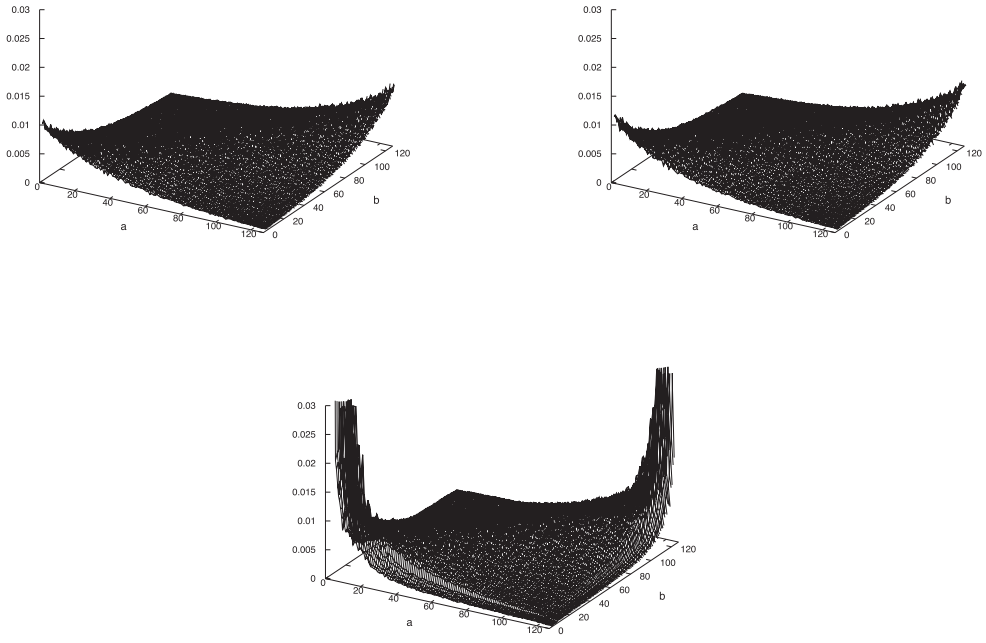

Fig. 9. The quantity $|\mathcal{A}_{ab}|$, defined by Eq. (2.16), is plotted for the bosonic model (top left) and for the model with fermionic contributions at $m_{\rm f} = 10$ (top right) and at $m_{\rm f} = 6$ (bottom), with $N = 128$, $n = 6$, $\gamma = 4$, $\tilde{d} = 5$, and $\xi = 12$.

However, we observed that the SO(9) symmetry remains unbroken in the bosonic model after removing the artifact of Lorentz boosts.

Adding the contributions from the fermionic matrices is not straightforward in the CLM. In order to avoid the singular drift problem of the CLM, we added a fermionic mass term (3.11) with the coefficient $m_{\rm f}$ taken to be sufficiently large. In the $m_{\rm f} \to \infty$ limit, the fermionic matrices decouple and one obtains the bosonic model. Within the region of $m_{\rm f}$ that allows us to avoid the singular drift problem, we did not see any qualitative difference from the bosonic model. Inspired by the SUSY deformation [62] of the type IIB matrix model, we therefore introduced some anisotropy in the bosonic mass term as Eq. (3.12), where the parameter ξ represents the anisotropy, which enables us to control the quantum fluctuations of the bosonic matrices preserving the SO($\tilde{d}$, 1) Lorentz symmetry. For $N = 128$, $\gamma = 4$, $m_{\rm f} = 6$, $\tilde{d} = 5$, and $\xi = 12$, we found that the configurations obtained by the simulations exhibit a prominent $(3+1)$D expanding behavior at late times, which implies the SSB from SO($\tilde{d}$) to SO(3).

Let us speculate on the mechanism for the emergence of an expanding $(3+1)$D spacetime. As we saw in the studies of the Euclidean model [7,16], the volume of space tends to be constant when the SSB occurs in the type IIB matrix model. Since the Pfaffian is a polynomial with respect to A_μ, it is conceivable that the modulus of the Pfaffian becomes larger for collapsed configurations due to the increase of the linear extension of space caused by this constant-volume property. On the other hand, when $m_{\rm f} = 0$, Pf$\mathcal{M}$ vanishes when A_μ is set to zero for all but two indices [10,98]. This strongly disfavors the emergence of spacetime with not greater than two spatial directions. In this discussion, we assume that the temporal matrix A_0 can be ignored since some of the spatial matrices become exponentially larger than the temporal matrix A_0 in the presence of the expanding behavior.

Downloaded from academic.oup.com/ptep/article/2026/9/093B06/8761727 by guest on 10 November 2026

In our simulations, we left the Lorentz symmetry unfixed, which resulted in random Lorentz boosts during the simulation. While we were able to remove the artifact of these Lorentz boosts by applying appropriate Lorentz transformations, our analysis cannot be fully justified since it breaks the holomorphicity required for the correct application of the CLM. We therefore think it important to fix the Lorentz symmetry nonperturbatively using the Faddeev–Popov procedure [75,76]. Simulation of this model by the CLM is ongoing (K. N. Anagnostopoulos et al., work in progress) at $N = 128$, and preliminary results suggest that our main conclusions remain the same.

In this work, we introduced the fermionic mass term to avoid the singular drift problem in the CLM and added some anisotropy in the bosonic mass term to mimic the SUSY deformation [62] of the type IIB matrix model. However, there are some important differences from the SUSY deformed model as we explain in Appendix B. Most importantly, $\gamma > 0$ requires pure imaginary $m_{\rm f}$ in the SUSY deformation, whereas we have chosen $m_{\rm f}$ to be real, which is more effective in avoiding the singular drift problem. (See Fig. 2.) Moreover, the cubic term in A_μ that has to be added in the action for the SUSY deformation becomes purely imaginary for $\gamma > 0$, which may cause some instability due to unbounded action. It is therefore quite nontrivial to simulate precisely the SUSY deformed model and see whether the $(3+1)$D expanding behavior can still be obtained. This is also underway (K. N. Anagnostopoulos et al., work in progress).

Last but not least, the CLM is not powerful enough to sample all the relevant saddle points and determine the most dominant one. For that, one needs to employ yet another promising approach to the sign problem, i.e. the Lefschetz thimble method [76]. While the computational cost is much larger than the CLM, it is certainly worth developing the method further and clarifying whether the most dominant saddle point is given by the $(3+1)$D expanding spacetime.

Acknowledgements

We would like to thank Kohta Hatakeyama and Yuta Ito for their participation at an earlier stage of this work. We are also grateful to Yuhma Asano and Naoyuki Yamamori for valuable discussions and comments. T.A. and A.T. were supported in part by Grants-in-Aid (Nos. 17K05425, and 18K03614, 21K03532, 25K07319, respectively) from the Japan Society for the Promotion of Science. This research was supported by MEXT as "Program for Promoting Researches on the Supercomputer Fugaku" (Simulation for basic science: approaching the new quantum era, JPMXP1020230411) and JICFuS. This work used computational resources of the supercomputer Fugaku provided by the RIKEN Center for Computational Science (Project IDs: hp210165, hp220174, hp230207, hp240213, hp250224), Oakbridge-CX provided by the University of Tokyo (Project IDs: hp200106, hp200130, hp210094, hp220074, hp230149), Grand Chariot provided by Hokkaido University (Project IDs: hp230149, hp240117), and Flow provided by Nagoya University (Project ID: hp250140) through the HPCI System Research Project. Numerical computations were also carried out on Yukawa-21 at YITP in Kyoto University, Flow in Nagoya University, and PC clusters in KEK Computing Research Center. This work was also supported by computational time granted by the Greek Research and Technology Network (GRNET) in the National HPC facility ARIS, under the project IDs LIIB2 and QCMM.

Funding

Open Access funding: SCOAP[3].

A. How to eliminate the artifact of Lorentz boosts

In this section, we explain how we determine the Lorentz transformations that remove the artifact of Lorentz boosts.

Downloaded from academic.oup.com/ptep/article/2026/9/093B06/8761727 by guest on 10 November 2026

The basic idea is to minimize the quantity

$$\mathcal{T} = \mathrm{Tr}\left(A_0^\dagger A_0\right) \tag{A.1}$$

with respect to Lorentz transformations for each sampled configuration. In practice, this can be achieved by iteratively applying the (1+1)D Lorentz transformation

$$\begin{pmatrix} A_0' \\ A_i' \end{pmatrix} = \begin{pmatrix} \cosh\sigma & \sinh\sigma \\ \sinh\sigma & \cosh\sigma \end{pmatrix} \begin{pmatrix} A_0 \\ A_i \end{pmatrix}, \tag{A.2}$$

where $i = 1, 2, \ldots, \tilde{d}$ and σ is a real parameter, to minimize the quantity (A.1) with respect to σ at each step.[16] To determine σ at each step, we substitute A_0' into Eq. (A.1), obtaining

$$\mathcal{T}' = \cosh^2\sigma\ \mathrm{Tr}\left(A_0^\dagger A_0\right) + \sinh^2\sigma\ \mathrm{Tr}\left(A_i^\dagger A_i\right) + 2\cosh\sigma\sinh\sigma\ \mathrm{Re}\,\mathrm{Tr}\left(A_0^\dagger A_i\right) . \tag{A.3}$$

Thus the problem reduces to minimizing

$$f(x) = a\cosh x + b\sinh x\,, \tag{A.4}$$

where $x = 2\sigma$ and

$$a = \mathrm{Tr}\left(A_0^\dagger A_0\right) + \mathrm{Tr}\left(A_i^\dagger A_i\right)\ , \quad b = 2\,\mathrm{Re}\,\mathrm{Tr}\left(A_0^\dagger A_i\right)\ . \tag{A.5}$$

The minimum, $\sqrt{a^2 - b^2}$, is achieved at $x = \tanh^{-1}(-b/a)$, where $|b/a| < 1$, which follows from the inequality

$$\mathrm{Tr}\,(A_0 \pm A_i)^\dagger (A_0 \pm A_i) \geq 0\,. \tag{A.6}$$

After the Lorentz transformation, the matrix A_0 is no longer diagonal. Therefore, we redefine α_a by diagonalizing A_0 as

$$A_0 \to U^{-1} A_0 U \equiv \tilde{A}_0\,, \tag{A.7}$$

where U is a general complex matrix,[17] and $\tilde{A}_0 = \mathrm{diag}(\alpha_1,\ \alpha_2,\ \ldots,\ \alpha_N)$ is a complex diagonal matrix with the ordering

$$\mathrm{Re}\,\alpha_1 < \mathrm{Re}\,\alpha_2 < \ldots < \mathrm{Re}\,\alpha_N\,. \tag{A.8}$$

We also transform the spatial matrices A_i accordingly as

$$A_i \to U^{-1} A_i U\,. \tag{A.9}$$

B. Relationship with the SUSY deformation

In this section, we discuss a connection between the deformations (3.11) and (3.12) used in simulating the Lorentzian model in this paper and the SUSY deformation of the type IIB matrix model [62]. Let us consider a deformed model S' of the type IIB matrix model with the action

$$S' = S + S_\gamma + S_{\mathrm{Myers}} + S_{m_{\mathrm{f}}}\,, \tag{B.1}$$

where S is the action of the original model defined in Eq. (2.1) and the terms S_γ and $S_{m_{\mathrm{f}}}$ are given by Eqs. (3.12) and (3.11), respectively. In addition to these terms, we also introduce the so-called Myers term

$$S_{\mathrm{Myers}} = -iN\zeta\,\mathrm{Tr}\,(A_7[A_8, A_9])\ . \tag{B.2}$$

[16] Note that the Lorentz symmetry SO(9, 1) is broken down to SO($\tilde{d}$, 1) in the deformed model, where $\tilde{d} = 5$ is chosen in our simulation. Hence the Lorentz transformation is performed with $\tilde{d} = 5$ in that case.

[17] Let us recall that the configurations A_μ generated by complex Langevin simulations are not Hermitian in general.

Downloaded from academic.oup.com/ptep/article/2026/9/093B06/8761727 by guest on 10 November 2026

By setting $\tilde{d} = 6, \xi = 3$ and

$$\gamma = -\frac{\mu^2}{32}, \qquad \zeta = \mu, \qquad m_{\rm f} = \frac{\mu}{4}$$

with μ being a real parameter, one obtains the SUSY deformation of the type IIB matrix model [62]. In that case, S' is indeed invariant under a deformed SUSY transformation

$$\begin{aligned} \delta A_\mu &= i\bar{\epsilon}\Gamma_\mu\psi \ , \\ \delta\psi &= \frac{i}{2}[A_\mu, A_\nu]\Gamma^{\mu\nu}\epsilon + \frac{\mu}{8}\{(\Gamma^\mu)^\dagger\Gamma^7(\Gamma^8)^\dagger\Gamma^9 + 2(\Gamma^7)^\dagger\Gamma^8(\Gamma^9)^\dagger\Gamma^\mu\}A_\mu\epsilon \ , \end{aligned} \tag{B.3}$$

where ϵ is a constant Grassmann-odd parameter transforming as a Majorana–Weyl spinor in (9+1) dimensions and $\Gamma^{\mu\nu} = -\{(\Gamma^\mu)^\dagger\Gamma^\nu - (\Gamma^\nu)^\dagger\Gamma^\mu\}/2$.

On the other hand, the model that we simulate in Section 4.2 corresponds to S' for $\tilde{d} = 5, \zeta = 0$ with γ, ξ, and $m_{\rm f}$ being real positive parameters. Thus, the deformation used in this work can be viewed as a generalization of the SUSY deformation of the type IIB matrix model.

The Euclidean version of the SUSY deformed model has attracted a lot of attention due to the discovery of holographic dual solutions in type IIB supergravity [63–65]. See also Refs. [66–69] for Monte Carlo studies of the Euclidean SUSY deformed model.

REFERENCES

[1] N. Ishibashi, H. Kawai, Y. Kitazawa, and A. Tsuchiya, Nucl. Phys. B **498**, 467 (1997) [arXiv:hep-th/9612115] [Search inSPIRE].
[2] H. Aoki, S. Iso, H. Kawai, Y. Kitazawa, and T. Tada, Prog. Theor. Phys. **99**, 713 (1998) [arXiv:hep-th/9802085] [Search inSPIRE].
[3] H. Aoki, S. Iso, H. Kawai, Y. Kitazawa, A. Tsuchiya, and T. Tada, Prog. Theor. Phys. Suppl. **134**, 47 (1999) [arXiv:hep-th/9908038] [Search inSPIRE].
[4] S. Iso and H. Kawai, Int. J. Mod. Phys. A **15**, 651 (2000) [arXiv:hep-th/9903217] [Search inSPIRE].
[5] H. Aoki, J. Nishimura, and A. Tsuchiya, J. High Energy Phys. **05**, 131 (2014) [arXiv:1401.7848 [hep-th]] [Search inSPIRE].
[6] K. Hatakeyama, A. Matsumoto, J. Nishimura, A. Tsuchiya, and A. Yosprakob, Prog. Theor. Exp. Phys. **2020**, 043B10 (2020) [arXiv:1911.08132 [hep-th]] [Search inSPIRE].
[7] J. Nishimura, T. Okubo, and F. Sugino, J. High Energy Phys. **10**, 135 (2011) [arXiv:1108.1293 [hep-th]] [Search inSPIRE].
[8] K. N. Anagnostopoulos, T. Azuma, and J. Nishimura, PoS **LATTICE2015**, 307 (2016) [arXiv:1509.05079 [hep-lat]] [Search inSPIRE].
[9] K. N. Anagnostopoulos, T. Azuma, Y. Ito, J. Nishimura, T. Okubo, and S, K. Papadoudis, J. High Energy Phys. **06**, 069 (2020) [arXiv:2002.07410 [hep-th]] [Search inSPIRE].
[10] J. Nishimura and G. Vernizzi, J. High Energy Phys. **04**, 015 (2000) [arXiv:hep-th/0003223] [Search inSPIRE].
[11] J. Nishimura and G. Vernizzi, Phys. Rev. Lett. **85**, 4664 (2000) [arXiv:hep-th/0007022] [Search in SPIRE].
[12] T. Hotta, J. Nishimura, and A. Tsuchiya, Nucl. Phys. B **545**, 543 (1999) [arXiv:hep-th/9811220] [Search inSPIRE].
[13] J. Ambjorn, K. N. Anagnostopoulos, W. Bietenholz, T. Hotta, and J. Nishimura, J. High Energy Phys. **07**, 011 (2000) [arXiv:hep-th/0005147] [Search inSPIRE].
[14] J. Ambjorn, K. N. Anagnostopoulos, W. Bietenholz, T. Hotta, and J. Nishimura, J. High Energy Phys. **07**, 013 (2000) [arXiv:hep-th/0003208] [Search inSPIRE].
[15] J. Nishimura, T. Okubo, and F. Sugino, Prog. Theor. Phys. **114**, 487 (2005) [arXiv:hep-th/0412194] [Search inSPIRE].
[16] T. Aoyama, J. Nishimura, and T. Okubo, Prog. Theor. Phys. **125**, 537 (2011) [arXiv:1007.0883 [hep-th]] [Search inSPIRE].
[17] K. N. Anagnostopoulos and J. Nishimura, Phys. Rev. D **66**, 106008 (2002) [arXiv:hep-th/0108041] [Search inSPIRE].

Downloaded from academic.oup.com/ptep/article/2026/9/093B06/8761727 by guest on 10 November 2026

[18] K. N. Anagnostopoulos, T. Azuma, and J. Nishimura, Phys. Rev. D **83**, 054504 (2011) [arXiv:1009.4504 [cond-mat.stat-mech]] [Search inSPIRE].
[19] K. N. Anagnostopoulos, T. Azuma, and J. Nishimura, J. High Energy Phys. **10**, 126 (2011) [arXiv:1108.1534 [hep-lat]] [Search inSPIRE].
[20] K. N. Anagnostopoulos, T. Azuma, and J. Nishimura, J. High Energy Phys. **11**, 009 (2013) [arXiv:1306.6135 [hep-th]] [Search inSPIRE].
[21] K. N. Anagnostopoulos, T. Azuma, Y. Ito, J. Nishimura, and S. K. Papadoudis, J. High Energy Phys. **02**, 151 (2018) [arXiv:1712.07562 [hep-lat]] [Search inSPIRE].
[22] K. N. Anagnostopoulos, T. Azuma, K. Hatakeyama, M. Hirasawa, Y. Ito, J. Nishimura, S. K. Papadoudis, and A. Tsuchiya, Eur. Phys. J. ST **232**, 3681 (2023) [arXiv:2210.17537 [hep-th]] [Search inSPIRE].
[23] S.-W. Kim, J. Nishimura, and A. Tsuchiya, Phys. Rev. Lett. **108**, 011601 (2012) [arXiv:1108.1540 [hep-th]] [Search inSPIRE].
[24] Y. Ito, S.-W. Kim, J. Nishimura, and A. Tsuchiya, PoS **LATTICE2013**, 341 (2014) [arXiv:1311.5579 [hep-lat]] [Search inSPIRE].
[25] Y. Ito, S.-W. Kim, Y. Koizuka, J. Nishimura, and A. Tsuchiya, Prog. Theor. Exp. Phys. **2014**, 083B01 (2014) [arXiv:1312.5415 [hep-th]] [Search inSPIRE].
[26] Y. Ito, J. Nishimura, and A. Tsuchiya, J. High Energy Phys. **11**, 070 (2015) [arXiv:1506.04795 [hep-th]] [Search inSPIRE].
[27] Y. Ito, J. Nishimura, and A. Tsuchiya, PoS **LATTICE2015**, 243 (2016) [arXiv:1512.01923 [hep-lat]] [Search inSPIRE].
[28] Y. Ito, J. Nishimura, and A. Tsuchiya, J. High Energy Phys. **03**, 143 (2017) [arXiv:1701.07783 [hep-th]] [Search inSPIRE].
[29] T. Aoki, M. Hirasawa, Y. Ito, J. Nishimura, and A. Tsuchiya, Prog. Theor. Exp. Phys. **2019**, 093B03 (2019) [arXiv:1904.05914 [hep-th]] [Search inSPIRE].
[30] G. Parisi, Phys. Lett. B **131**, 393 (1983).
[31] J. R. Klauder, Phys. Rev. A **29**, 2036 (1984).
[32] J. Nishimura and A. Tsuchiya, J. High Energy Phys. **06**, 077 (2019) [arXiv:1904.05919 [hep-th]] [Search inSPIRE].
[33] S.-W. Kim, J. Nishimura, and A. Tsuchiya, Phys. Rev. D **86**, 027901 (2012) [arXiv:1110.4803 [hep-th]] [Search inSPIRE].
[34] S.-W. Kim, J. Nishimura, and A. Tsuchiya, J. High Energy Phys. **10**, 147 (2012) [arXiv:1208.0711 [hep-th]] [Search inSPIRE].
[35] H. C. Steinacker, Phys. Lett. B **827**, 136946 (2022) [arXiv:2110.03936 [hep-th]] [Search inSPIRE].
[36] H. C. Steinacker, J. High Energy Phys. **05**, 129 (2023) [arXiv:2303.08012 [hep-th]] [Search inSPIRE].
[37] E. Battista and H. C. Steinacker, J. High Energy Phys. **01**, 125 (2024) [arXiv:2310.11126 [hep-th]] [Search inSPIRE].
[38] K. Kumar and H. C. Steinacker, Classical Quantum Gravity **41**, 185007 (2024) [arXiv:2312.01317 [hep-th]] [Search inSPIRE].
[39] H. C. Steinacker, Quantum Geometry, Matrix Theory, and Gravity (Cambridge University Press, Cambridge, UK, 2024).
[40] A. Manta, H. C. Steinacker, and T. Tran, J. High Energy Phys. **02**, 031 (2025) [arXiv:2411.02598 [hep-th]] [Search inSPIRE].
[41] A. Manta and H. C. Steinacker, J. Phys. A **58**, 175204 (2025) [arXiv:2502.02498 [hep-th]] [Search inSPIRE].
[42] A. Manta and H. C. Steinacker, J. High Energy Phys. **02**, 062 (2026) [arXiv:2509.24753 [hep-th]] [Search inSPIRE].
[43] F. R. Klinkhamer, Prog. Theor. Exp. Phys. **2021**, 063 (2021) [arXiv:2009.06525 [hep-th]] [Search inSPIRE].
[44] S. Brahma, R. Brandenberger, and S. Laliberte, J. High Energy Phys. **03**, 067 (2022) [arXiv:2107.11512 [hep-th]] [Search inSPIRE].
[45] S. Brahma, R. Brandenberger, and S. Laliberte, J. High Energy Phys. **09**, 031 (2022) [arXiv:2206.12468 [hep-th]] [Search inSPIRE].
[46] S. Brahma, R. Brandenberger, and S. Laliberte, MDPI Physics **5**, 1 (2023) [arXiv:2210.07288 [hep-th]] [Search inSPIRE].

Downloaded from academic.oup.com/ptep/article/2026/9/093B06/8761727 by guest on 10 November 2026

[47] F. R. Klinkhamer, Classical Quantum Gravity **40**, 124001 (2023) [arXiv:2212.00709 [hep-th]] [Search inSPIRE].
[48] S. Laliberte and S. Brahma, J. High Energy Phys. **11**, 161 (2023) [arXiv:2304.10509 [hep-th]] [Search inSPIRE].
[49] R. Brandenberger and J. Pasiecznik, Phys. Rev. D **112**, 026006 (2025) [arXiv:2409.00254 [hep-th]] [Search inSPIRE].
[50] K. Hattori, Y. Mizuno, and A. Tsuchiya, Prog. Theor. Exp. Phys. **2024**, 123B06 (2024) [arXiv:2410.13414 [hep-th]] [Search inSPIRE].
[51] J. Gohara and A. Sako, J. Math. Phys. **67**, 022301 (2026) [arXiv:2503.24060 [hep-th]] [Search inSPIRE].
[52] P.-M. Ho, H. Kawai, and H. C. Steinacker, J. High Energy Phys. **02**, 070 (2026) [arXiv:2509.06646 [hep-th]] [Search inSPIRE].
[53] C. Gaß and H. C. Steinacker, Phys. Rev. D **113**, 024050 (2026) [arXiv:2510.21283 [hep-th]] [Search inSPIRE].
[54] H. Liao and R. Maeta, Phys. Rev. D **114**, 026021 (2026) [arXiv:2512.03161 [hep-th]] [Search inSPIRE].
[55] H. C. Steinacker, J. High Energy Phys. **04**, 044 (2026) [arXiv:2601.08031 [hep-th]] [Search inSPIRE].
[56] G. Aarts, F. A. James, E. Seiler, and I.-O. Stamatescu, Phys. Lett. B **687**, 154 (2010) [arXiv:0912.0617 [hep-lat]] [Search inSPIRE].
[57] G. Aarts, E. Seiler, and I.-O. Stamatescu, Phys. Rev. D **81**, 054508 (2010) [arXiv:0912.3360 [hep-lat]] [Search inSPIRE].
[58] G. Aarts, F. A. James, E. Seiler, and I.-O. Stamatescu, Eur. Phys. J. C **71**, 1756 (2011) [arXiv:1101.3270 [hep-lat]] [Search inSPIRE].
[59] J. Nishimura and S. Shimasaki, Phys. Rev. D **92**, 011501 (2015) [arXiv:1504.08359 [hep-lat]] [Search inSPIRE].
[60] K. Nagata, J. Nishimura, and S. Shimasaki, Prog. Theor. Exp. Phys. **2016**, 013B01 (2016) [arXiv:1508.02377 [hep-lat]] [Search inSPIRE].
[61] K. Nagata, J. Nishimura, and S. Shimasaki, Phys. Rev. D **94**, 114515 (2016) [arXiv:1606.07627 [hep-lat]] [Search inSPIRE].
[62] G. Bonelli, J. High Energy Phys. **08**, 022 (2002) [arXiv:hep-th/0205213] [Search inSPIRE].
[63] S. A. Hartnoll and J. Liu, J. High Energy Phys. **03**, 060 (2025) [arXiv:2409.18706 [hep-th]] [Search inSPIRE].
[64] S. Komatsu, A. Martina, J. Penedones, A. Vuignier, and X. Zhao, J. High Energy Phys. **12**, 029 (2025) [arXiv:2410.18173 [hep-th]] [Search inSPIRE].
[65] S. Komatsu, A. Martina, J. Penedones, A. Vuignier, and X. Zhao, J. High Energy Phys. **12**, 030 (2025) [arXiv:2411.18678 [hep-th]] [Search inSPIRE].
[66] A. Kumar, A. Joseph, and P. Kumar, PoS **LATTICE2022**, 213 (2023) [arXiv:2209.10494 [hep-lat]] [Search inSPIRE].
[67] A. Kumar, A. Joseph, and P. Kumar, Springer Proc. Phys. **304**, 1201 (2024) [arXiv:2308.03607 [hep-lat]] [Search inSPIRE].
[68] S. A. Hartnoll and J. Liu, SciPost Phys. **19**, 099 (2025) [arXiv:2504.06481 [hep-th]] [Search inSPIRE].
[69] C.-Y. Chou, J. Nishimura, and C.-T. Wang, Phys. Rev. Lett. **135**, 221601 (2025) [arXiv:2507.18472 [hep-th]] [Search inSPIRE].
[70] K. Hatakeyama, K. Anagnostopoulos, T. Azuma, M. Hirasawa, Y. Ito, J. Nishimura, S. Papadoudis, and A. Tsuchiya, PoS **LATTICE2021**, 341 (2022) [arXiv:2112.15368 [hep-lat]] [Search inSPIRE].
[71] K. Hatakeyama, K. Anagnostopoulos, T. Azuma, M. Hirasawa, Y. Ito, J. Nishimura, S. Papadoudis, and A. Tsuchiya, arXiv:2201.13200 [hep-th] [Search inSPIRE].
[72] J. Nishimura, PoS **CORFU2021**, 255 (2022) [arXiv:2205.04726 [hep-th]] [Search inSPIRE].
[73] M. Hirasawa, K. N. Anagnostopoulos, T. Azuma, K. Hatakeyama, J. Nishimura, S. K. Papadoudis, and A. Tsuchiya, PoS **LATTICE2022**, 371 (2023) [arXiv:2212.10127 [hep-lat]] [Search inSPIRE].
[74] M. Hirasawa, K. N. Anagnostopoulos, T. Azuma, K. Hatakeyama, J. Nishimura, S. Papadoudis, and A. Tsuchiya, PoS **CORFU2023**, 257 (2024) [arXiv:2407.03491 [hep-th]] [Search inSPIRE].
[75] Y. Asano, J. Nishimura, W. Piensuk, and N. Yamamori, Phys. Rev. Lett. **134**, 041603 (2025) [arXiv:2404.14045 [hep-th]] [Search inSPIRE].

Downloaded from academic.oup.com/ptep/article/2026/9/093B06/8761727 by guest on 10 November 2026

[76] C.-Y. Chou, J. Nishimura, and A. Tripathi, Phys. Rev. Lett. **134**, 211601 (2025) [arXiv:2501.17798 [hep-th]] [Search inSPIRE].
[77] H. C. Steinacker, J. High Energy Phys. **02**, 033 (2018) [arXiv:1709.10480 [hep-th]] [Search inSPIRE].
[78] M. Scherzer, E. Seiler, D. Sexty, and I.-O. Stamatescu, Phys. Rev. D **99**, 014512 (2019) [arXiv:1808.05187 [hep-lat]] [Search inSPIRE].
[79] M. Scherzer, E. Seiler, D. Sexty, and I. O. Stamatescu, Phys. Rev. D **101**, 014501 (2020) [arXiv:1910.09427 [hep-lat]] [Search inSPIRE].
[80] E. Seiler, D. Sexty, and I.-O. Stamatescu, Phys. Rev. D **109**, 014509 (2024) [arXiv:2304.00563 [hep-lat]] [Search inSPIRE].
[81] M. W. Hansen, M. Mandl, E. Seiler, and D. Sexty, Phys. Rev. D **111**, 074502 (2025) [arXiv:2412.17137 [hep-lat]] [Search inSPIRE].
[82] M. Mandl, E. Seiler, and D. Sexty, J. Phys. A **58**, 495202 (2025) [arXiv:2508.14512 [hep-lat]] [Search inSPIRE].
[83] M. Mandl, JHEP **08**, 110 (2026) [arXiv:2604.12388 [hep-lat]] [Search inSPIRE].
[84] D. Sexty, Phys. Lett. B **729**, 108 (2014) [arXiv:1307.7748 [hep-lat]] [Search inSPIRE].
[85] Z. Fodor, S. D. Katz, D. Sexty, and C. Török, Phys. Rev. D **92**, 094516 (2015) [arXiv:1508.05260 [hep-lat]] [Search inSPIRE].
[86] D. Sexty, Phys. Rev. D **100**, 074503 (2019) [arXiv:1907.08712 [hep-lat]] [Search inSPIRE].
[87] M. Scherzer, D. Sexty, and I. O. Stamatescu, Phys. Rev. D **102**, 014515 (2020) [arXiv:2004.05372 [hep-lat]] [Search inSPIRE].
[88] Y. Ito, H. Matsufuru, Y. Namekawa, J. Nishimura, S. Shimasaki, A. Tsuchiya, and S. Tsutsui, J. High Energy Phys. **10**, 144 (2020) [arXiv:2007.08778 [hep-lat]] [Search inSPIRE].
[89] S. Tsutsui, Y. Asano, Y. Ito, H. Matsufuru, Y. Namekawa, J. Nishimura, S. Shimasaki, and A. Tsuchiya, J. High Energy Phys. **10**, 108 (2025) [arXiv:2505.06551 [hep-lat]] [Search inSPIRE].
[90] Y. Asano, Y. Ito, J. Nishimura, and N. Shimizu, Phys. Rev. C **114**, 034319 (2026) [arXiv:2508.15116 [nucl-th]] [Search inSPIRE].
[91] M. Fukugita, Y. Oyanagi, and A. Ukawa, Phys. Rev. D **36**, 824 (1987).
[92] E. Seiler, D. Sexty, and I.-O. Stamatescu, Phys. Lett. B **723**, 213 (2013) [arXiv:1211.3709 [hep-lat]] [Search inSPIRE].
[93] K. Nagata, J. Nishimura, and S. Shimasaki, J. High Energy Phys. **07**, 073 (2016) [arXiv:1604.07717 [hep-lat]] [Search inSPIRE].
[94] A. Mollgaard and K. Splittorff, Phys. Rev. D **88**, 116007 (2013) [arXiv:1309.4335 [hep-lat]] [Search inSPIRE].
[95] G. Aarts, E. Seiler, D. Sexty, and I.-O. Stamatescu, J. High Energy Phys. **05**, 044 (2017); **01**, 128 (2018) [erratum] [arXiv:1701.02322 [hep-lat]] [Search inSPIRE].
[96] D. E. Berenstein, J. M. Maldacena, and H. S. Nastase, J. High Energy Phys. **04**, 013 (2002) [arXiv:hep-th/0202021] [Search inSPIRE].
[97] F. Attanasio and B. Jäger, Eur. Phys. J. C **79**, 16 (2019) [arXiv:1808.04400 [hep-lat]] [Search inSPIRE].
[98] W. Krauth, H. Nicolai, and M. Staudacher, Phys. Lett. B **431**, 31 (1998) [arXiv:hep-th/9803117] [Search inSPIRE].

Downloaded from academic.oup.com/ptep/article/2026/9/093B06/8761727 by guest on 10 November 2026

© The Author(s) 2026. Published by Oxford University Press on behalf of the Physical Society of Japan. This is an Open Access article distributed under the terms of the Creative Commons Attribution License (https://creativecommons.org/licenses/by/4.0/), which permits unrestricted reuse, distribution, and reproduction in any medium, provided the original work is properly cited.
Funded by SCOAP[3]